

## **Three-dimensional numerical simulation of density-dependent groundwater flow and salt transport due to groundwater pumping in a heterogeneous and true anisotropic coastal aquifer system**

**JU-HYUN PARK, CHAN-SUNG OH & JUN-MO KIM**

*School of Earth and Environmental Sciences, Seoul National University, Seoul 151-742, Korea  
[junmokim@snu.ac.kr](mailto:junmokim@snu.ac.kr)*

**Abstract** A series of three-dimensional numerical simulations using a multidimensional hydrodynamic dispersion numerical model is performed to analyse seawater intrusion under groundwater pumping in an unsaturated fractured porous coastal aquifer system, which is heterogeneous and true anisotropic. The numerical simulation results show that such heterogeneity and true anisotropy have significant effects on spatial and temporal distributions of density-dependent groundwater flow and salt transport. Therefore, it may be concluded that both heterogeneity and true anisotropy must be properly considered when more rigorous and reasonable predictions of long-term density-dependent groundwater flow and salt transport induced by groundwater pumping are to be obtained for the optimal management of coastal groundwater resources.

**Key words** fractured porous coastal aquifer system; heterogeneity; true anisotropy; groundwater pumping; seawater intrusion; hydrodynamic dispersion; numerical simulation

### **INTRODUCTION**

Groundwater has been pumped indiscreetly and excessively from coastal aquifers for various human activities as the population has grown throughout the world, especially in Asia. As a result, extensive coastal groundwater depletion and salinization have occurred under intensive seawater intrusion, and thus the sustainability of coastal groundwater resources has become a significant issue in coastal areas and even in the adjacent inland areas.

Various hydrodynamic dispersion numerical models have been developed on the basis of the fully coupled governing equations for groundwater flow and solute transport and then used as useful tools to simulate seawater intrusion and related phenomena for the management of coastal groundwater resources (see Bear *et al.*, 1999; Cheng & Ouazar, 2004). However, numerical simulations of seawater intrusion in heterogeneous and true anisotropic fractured porous coastal aquifer systems, which contain complex spatial distributions of geological media (rock masses), and each of the geological media has joints or joint sets of various orientations, have not yet been performed seriously.

The objectives of this study are to simulate density-dependent groundwater flow and salt transport due to groundwater pumping in an unsaturated heterogeneous and true anisotropic coastal aquifer system using a multidimensional hydrodynamic dispersion numerical model and to evaluate the effects of heterogeneity and true

anisotropy on such coupled groundwater flow and salt transport phenomena. From a practical point of view, such a quantitative understanding of the effects of heterogeneity and true anisotropy may suggest improved guidelines for planning, designing, assessing, and modifying groundwater pumping schemes for the optimal management of coastal groundwater resources.

## NUMERICAL MODEL

The hydrodynamic dispersion numerical model used in this study is COFAT3D (Kim & Yeh, 2004), which has been developed from 3DFEMFAT (Yeh *et al.*, 1994). This numerical model is a general multidimensional hybrid Lagrangian-Eulerian finite element model and can simulate density-dependent groundwater flow and solute transport in saturated–unsaturated porous, fractured, and fractured porous geological media, which are heterogeneous and true anisotropic. This numerical model uses the adaptive finite difference time-stepping scheme for transient problems, the incremental Picard method for coupled nonlinear problems, and one of four conventional and preconditioned conjugate gradient (PCG) iterative methods for matrix solutions. In this study, the linearized groundwater flow and solute transport matrix equations are solved sequentially by the incomplete Cholesky LU decomposed preconditioned conjugate gradient (ICPCG) iterative method, while the convergence criteria for pressure head and seawater-normalized solute concentration are set equal to  $10^{-3}$  m and  $10^{-3}$  for nonlinear iterations and  $10^{-4}$  m and  $10^{-4}$  for linear iterations.

## NUMERICAL SIMULATIONS

### Coastal aquifer system

The coastal aquifer system considered in this study is located on the western coast of Korea and is composed of Quaternary alluvial layers underlain by Precambrian gneiss and Cretaceous quartz monzonite, rhyolitic tuff, Kyokpori Formation (conglomerate, sandstone, and shale), and rhyolite with a major fault as shown in Fig. 1 (Korea Institute of Geoscience and Mineral Resources, 1997; Kim, 2000). Such geological rock masses (media) and faults do not only have irregular thicknesses and boundaries but also contain numerous joints and bedding planes of various orientations. Thus the coastal aquifer system is hydrogeologically heterogeneous and true anisotropic.

Groundwater has been pumped indiscreetly from the overlying alluvial layers and even from the underlying bedrocks for various agricultural and municipal activities since the late 1990s. As a result, seawater intrusion has intensified, and it has caused extensive groundwater depletion and salinization. In order to predict and analyse the seawater intrusion under groundwater pumping in such a heterogeneous and true anisotropic coastal aquifer system, a series of three-dimensional numerical simulations of density-dependent groundwater flow and salt transport has often been requested.

The material properties of the geological media and fault, which compose the coastal aquifer system, are obtained from a variety of geological surveys and hydrogeological tests and are summarized in Table 1, and the characteristics of the joint

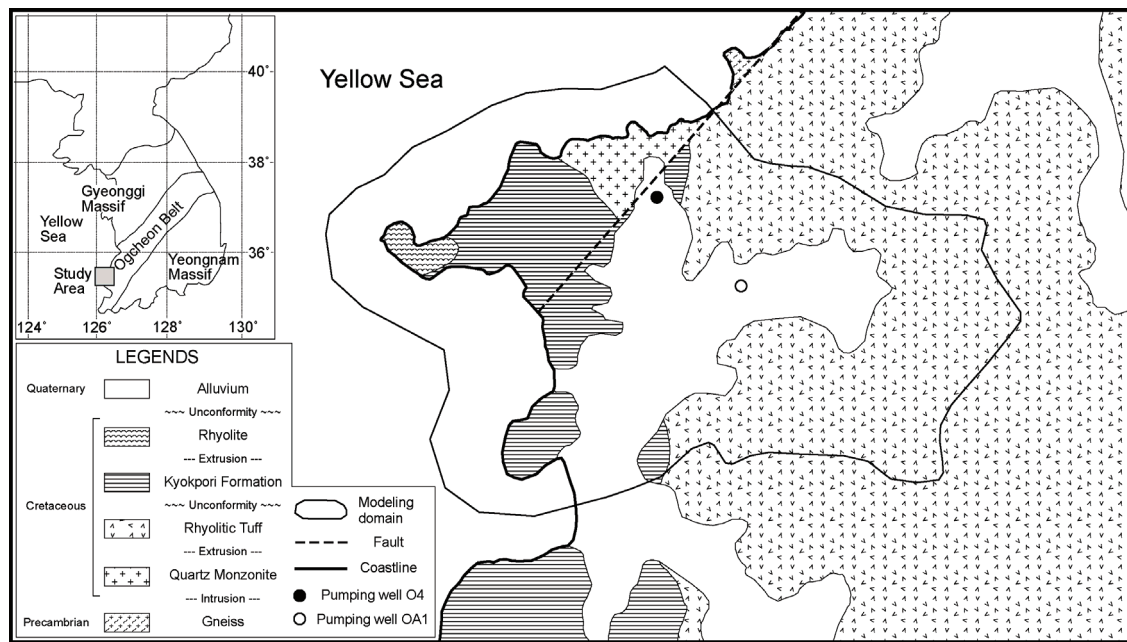


**Fig. 1** Location and geological maps of the study area. The horizontal extent of the coastal aquifer system modelled in this study is outlined by a thin solid line. The pumping wells O4 and OA1 are marked by the full and open circles, respectively.

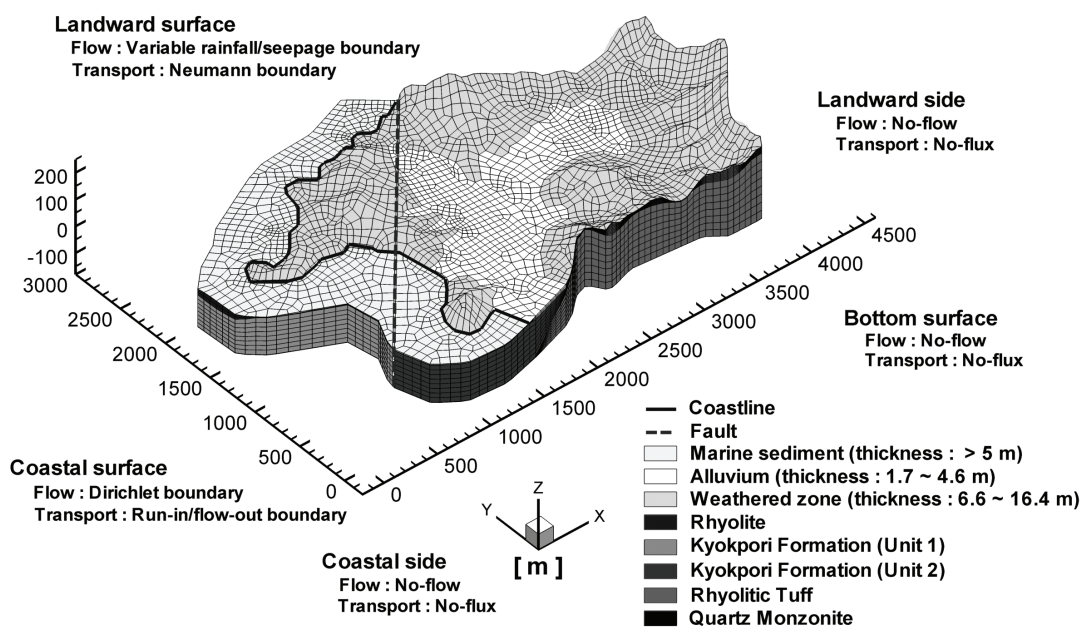
**Table 1** Material properties of the geological media and fault.

Property	Quartz monzonite	Rhyolitic tuff	Kyokpori Formation (Unit 1)	Kyokpori Formation (Unit 2)	Rhyolite	Weathered zone	Alluvium and marine sediment	Fault
Porosity	$1.60 \times 10^{-2}$	$8.50 \times 10^{-2}$	$2.60 \times 10^{-2}$	$2.60 \times 10^{-2}$	$1.00 \times 10^{-1}$	$1.90 \times 10^{-1}$	$4.30 \times 10^{-1}$	$1.90 \times 10^{-1}$
Sat. hydraulic conductivity (m/s)	$2.50 \times 10^{-12}$	$2.16 \times 10^{-10}$	$1.10 \times 10^{-6}$	$1.01 \times 10^{-6}$	$4.00 \times 10^{-7}$	$2.10 \times 10^{-5}$	$2.88 \times 10^{-4}$	$6.01 \times 10^{-7}$
Dry bulk density ( $\text{kg}/\text{m}^3$ )	$2.61 \times 10^3$	$2.40 \times 10^3$	$2.58 \times 10^3$	$2.58 \times 10^3$	$2.31 \times 10^3$	$2.15 \times 10^3$	$1.52 \times 10^3$	$2.15 \times 10^3$
Longitudinal dispersivity (m)	15.80	15.80	15.80	15.80	15.80	31.60	31.60	31.60
Transverse dispersivity (m)	1.58	1.58	1.58	1.58	1.58	3.16	3.16	3.16
Residual water saturation	$8.64 \times 10^{-3}$	$4.59 \times 10^{-2}$	$8.60 \times 10^{-3}$	$8.60 \times 10^{-3}$	$6.93 \times 10^{-2}$	$7.35 \times 10^{-2}$	$1.05 \times 10^{-1}$	$8.94 \times 10^{-2}$
Unsaturated hydraulic parameters of van Genuchten's (1980) model								
$\alpha_v$ (1/m)	0.50	0.50	2.00	2.00	2.70	7.50	14.50	1.60
$n_v$	1.09	1.09	1.41	1.41	1.23	1.89	2.68	1.37

sets in the geological media and fault are summarized in Table 2 (Kim, 2006). The tortuosity is set equal to 0.41 assuming that the solid particles which compose the geologic media are spherical in shape. The compressibility of water is set equal to  $4.40 \times 10^{-10} \text{ m}^2/\text{N}$ , the density of fresh water is set equal to  $1000 \text{ kg}/\text{m}^3$ , and the dynamic viscosity of water is set equal to  $1.00 \times 10^{-3} \text{ kg m s}^{-1}$ . The density of seawater is set equal to  $1025 \text{ kg}/\text{m}^3$ ; that is, the density difference ratio is set equal to 0.025. The molecular diffusion coefficient of salt in water is set equal to  $1.68 \times 10^{-9} \text{ m}^2/\text{s}$  (Freeze & Cherry, 1979; Domenico & Schwartz, 1990; Fetter, 1994).

**Table 2** Characteristics of the joint sets in the geological media and fault.

Geologic media	Joint set	Strike	Dip	Aperture (m)	Spacing (m)
Quartz monzonite	Set 1	N76°W	4°W	$3.00 \times 10^{-5}$	$3.75 \times 10^{-1}$
	Set 2	N52°W	64°W	$6.00 \times 10^{-5}$	$2.64 \times 10^{-1}$
	Set 3	N88°W	88°E	$6.00 \times 10^{-5}$	$2.18 \times 10^{-1}$
Rhyolitic tuff	Set 1	N9°E	10°W	$3.00 \times 10^{-5}$	$2.03 \times 10^{-1}$
	Set 2	N25°W	80°E	$6.00 \times 10^{-5}$	$2.32 \times 10^{-1}$
	Set 3	N72°E	82°E	$6.00 \times 10^{-5}$	$1.92 \times 10^{-1}$
Kyokpori Formation (Unit 1)	Matrix	N47°E	14°W		
	Set 1 (bedding plane)	N47°E	14°W	$3.00 \times 10^{-5}$	$2.70 \times 10^{-1}$
	Set 2	N10°E	79°W	$6.00 \times 10^{-5}$	$3.38 \times 10^{-1}$
	Set 3	N84°W	85°W	$6.00 \times 10^{-5}$	$2.71 \times 10^{-1}$
Kyokpori Formation (Unit 2)	Matrix	N35°E	7°W		
	Set 1 (bedding plane)	N35°E	7°W	$3.00 \times 10^{-5}$	$2.20 \times 10^{-1}$
	Set 2	N49°E	90°	$6.00 \times 10^{-5}$	$3.10 \times 10^{-1}$
	Set 3	N58°W	85°W	$6.00 \times 10^{-5}$	$6.00 \times 10^{-1}$
	Set 4	N16°E	72°W	$6.00 \times 10^{-5}$	$5.32 \times 10^{-1}$
Rhyolite	Set 1	N84°E	82°W	$5.00 \times 10^{-5}$	$1.25 \times 10^{-1}$
	Set 2	N10°E	90°	$5.00 \times 10^{-5}$	$1.20 \times 10^{-1}$
Fault	Matrix	N49°E	90°		
	Set 1	N49°E	90°	$1.00 \times 10^{-4}$	$1.25 \times 10^0$
	Set 2	N49°E	90°	$2.00 \times 10^{-4}$	$2.00 \times 10^{-1}$
	Set 3	N49°E	90°	$2.00 \times 10^{-4}$	$6.67 \times 10^{-2}$

**Fig. 2** Finite element mesh and boundary conditions of the coastal aquifer system used in the numerical simulations. The  $x$ ,  $y$  and  $z$  axes are aligned toward the east, north, and zenith, respectively.

The horizontal landward and coastal side boundaries of the coastal aquifer system modelled in this study are determined considering onshore mountain ridges and offshore topographies beyond the coastline, respectively, and are outlined by a thin solid line as shown in Fig. 1. The bottom boundary of the coastal aquifer system is horizontally flat and is located at a depth of 150 m b.s.l. The coastal aquifer system with these horizontal and bottom boundaries is discretized into 53 314 irregular hexahedral elements with 58 240 nodes as shown in Fig. 2. The boundary conditions for the coastal aquifer system are also summarized in Fig. 2. The net annual average rainfall rate is set equal to 20% of the annual average rainfall rate of 1209 mm/year considering evaporation and transpiration (Korea Meteorological Administration, 1971–2000).

## RESULTS AND ANALYSES

In order to obtain initial steady-state spatial distributions of density-dependent groundwater flow and salt transport in the coastal aquifer system before groundwater pumping, a steady-state numerical simulation is performed first, and its results are illustrated in Fig. 3. Figure 3 clearly shows that the above-mentioned heterogeneity and true anisotropy, especially the major fault, as well as the topography and unsaturated zone, have significant effects on the spatial distributions of hydraulic head, seawater-normalized salt concentration, groundwater flow flux, and seawater-normalized salt transport flux before groundwater pumping. As shown in Fig. 3, the major fault acts as a highly permeable conduit along it but behaves as a less permeable barrier across it. On the other hand, as shown in Fig. 3(d), the measured and simulated transition (or mixing) zones (in other words, interfaces or salt water fronts) between fresh water and salt water before groundwater pumping are reasonably well matched recognizing that there is no calibration procedure involved in this steady-state numerical simulation. Therefore, the results from this steady-state numerical simulation are expected to represent the field behaviour closely and adequately. Here, the measured transition zones are inferred from an electrical resistivity (ER) sounding (Line 1) and an electrical conductivity (EC) logging (Line 2).

In order to obtain spatial and temporal distributions of density-dependent groundwater flow and salt transport in the coastal aquifer system during groundwater pumping at two different pumping wells O4 and OA1 (see Fig. 1) and two different pumping rates (100 and 400 m<sup>3</sup>/day), four different transient-state numerical simulations are then performed using their initial steady-state spatial distributions (i.e. Fig. 3) as initial conditions, and their results are illustrated in Figs 4–9 and are compared with Fig. 3(a)–(f), respectively. Figures 4–9 clearly show that the above-mentioned heterogeneity and true anisotropy, especially the major fault, as well as the topography and unsaturated zone, have significant effects on the spatial distributions of hydraulic head, seawater-normalized salt concentration, groundwater flow flux, and seawater-normalized salt transport flux during groundwater pumping. Such effects of heterogeneity and true anisotropy become more prominent when groundwater is pumped from Well O4 since it is closer to the major fault than Well OA1. It is also certain that groundwater depletion and salinization become intensive and extensive as the pumping rate increases at either pumping well. As shown in Fig. 10, the hydraulic

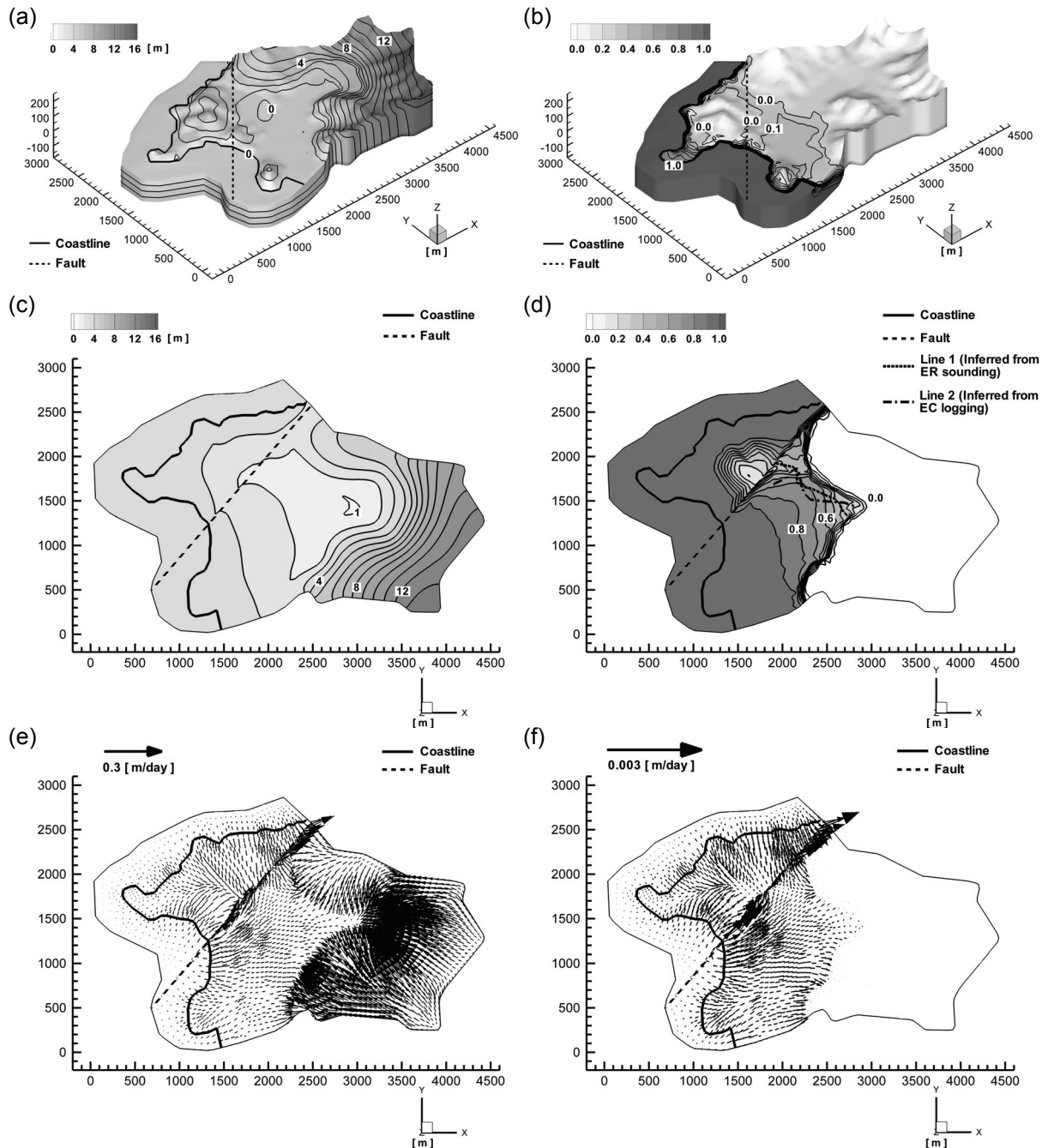


**Fig. 3** Initial steady-state spatial distributions of: (a) hydraulic head (m), (b) normalized salt concentration, (c) hydraulic head (m) at the bottom boundary, (d) normalized salt concentration at the bottom boundary, (e) groundwater flow flux (m/day) at the bottom boundary, and (f) normalized salt transport flux (m/day) at the bottom boundary before groundwater pumping in the coastal aquifer system. The contour intervals of hydraulic head and normalized salt concentration are 1 m and 0.1, respectively.

head reaches its final steady-state condition much faster (in about 1 day) than the seawater-normalized salt concentration (after more than 50 years) at either pumping well. This results from salt transport under hydrodynamic dispersion as well as advection. In addition, the seawater-normalized salt concentration at Well O4 still

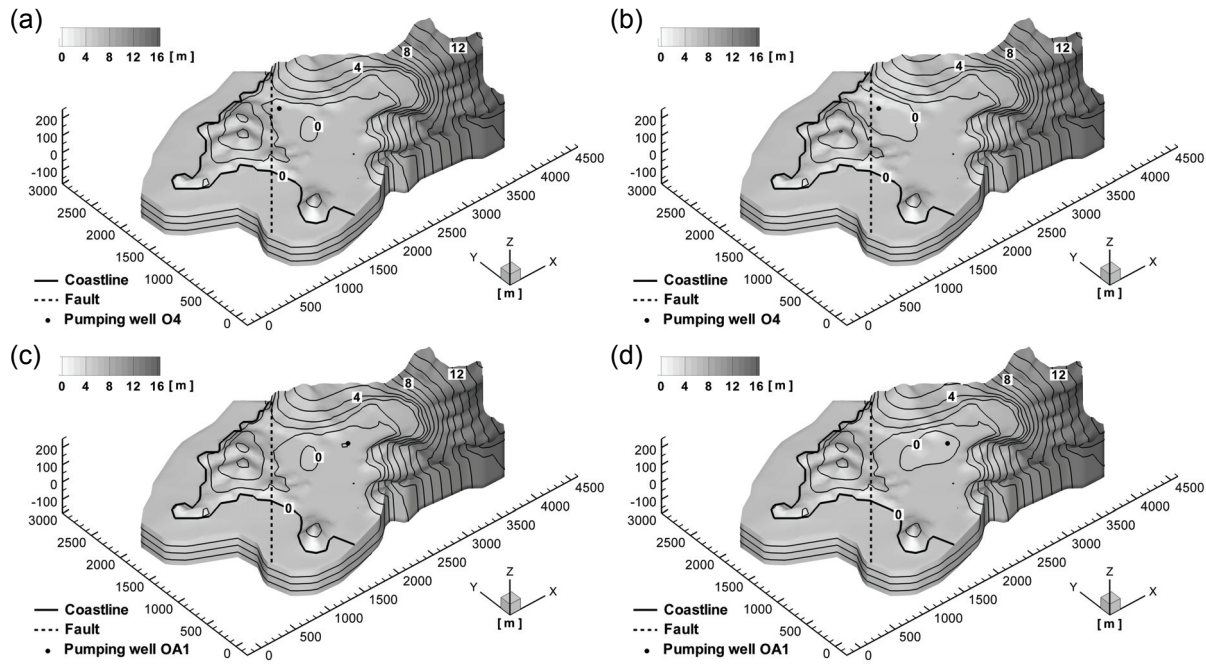


**Fig. 4** Final steady-state spatial distributions of hydraulic head (m) during groundwater pumping at rates of: (a) 100 m<sup>3</sup>/day at Well O4, (b) 400 m<sup>3</sup>/day at Well O4, (c) 100 m<sup>3</sup>/day at Well OA1, and (d) 400 m<sup>3</sup>/day at Well OA1 in the coastal aquifer system. The contour interval of hydraulic head is 1 m.

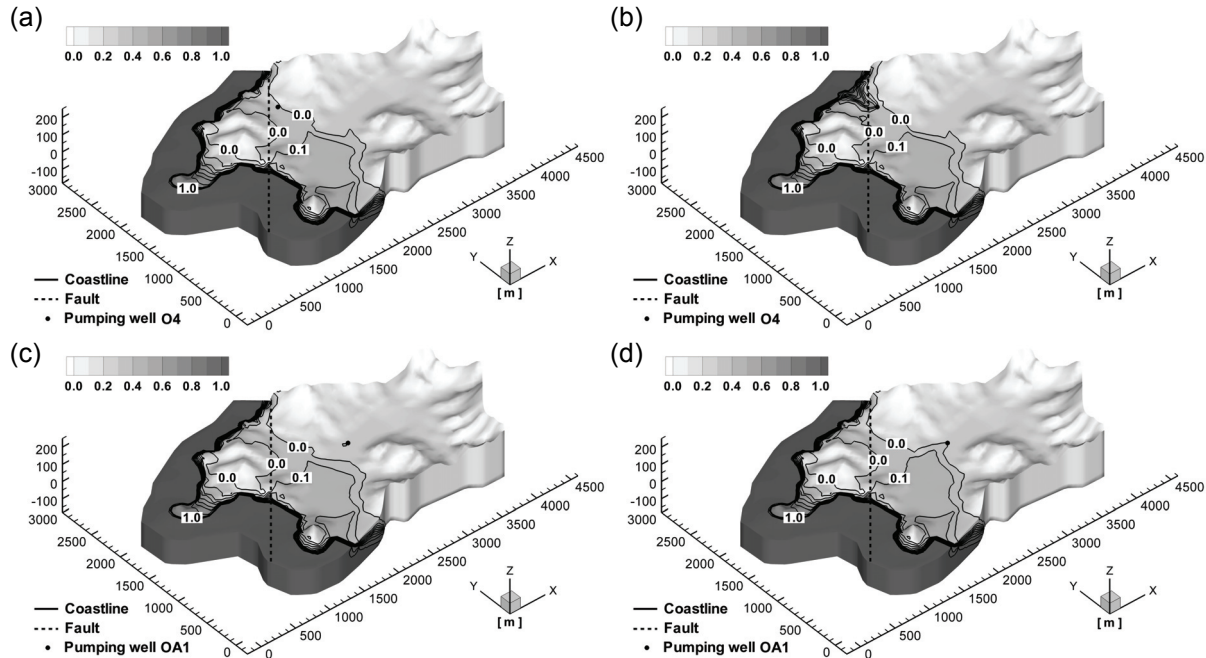


**Fig. 5** Final steady-state spatial distributions of normalized salt concentration during groundwater pumping at rates of: (a) 100 m<sup>3</sup>/day at Well O4, (b) 400 m<sup>3</sup>/day at Well O4, (c) 100 m<sup>3</sup>/day at Well OA1, and (d) 400 m<sup>3</sup>/day at Well OA1 in the coastal aquifer system. The contour interval of normalized salt concentration is 0.1.

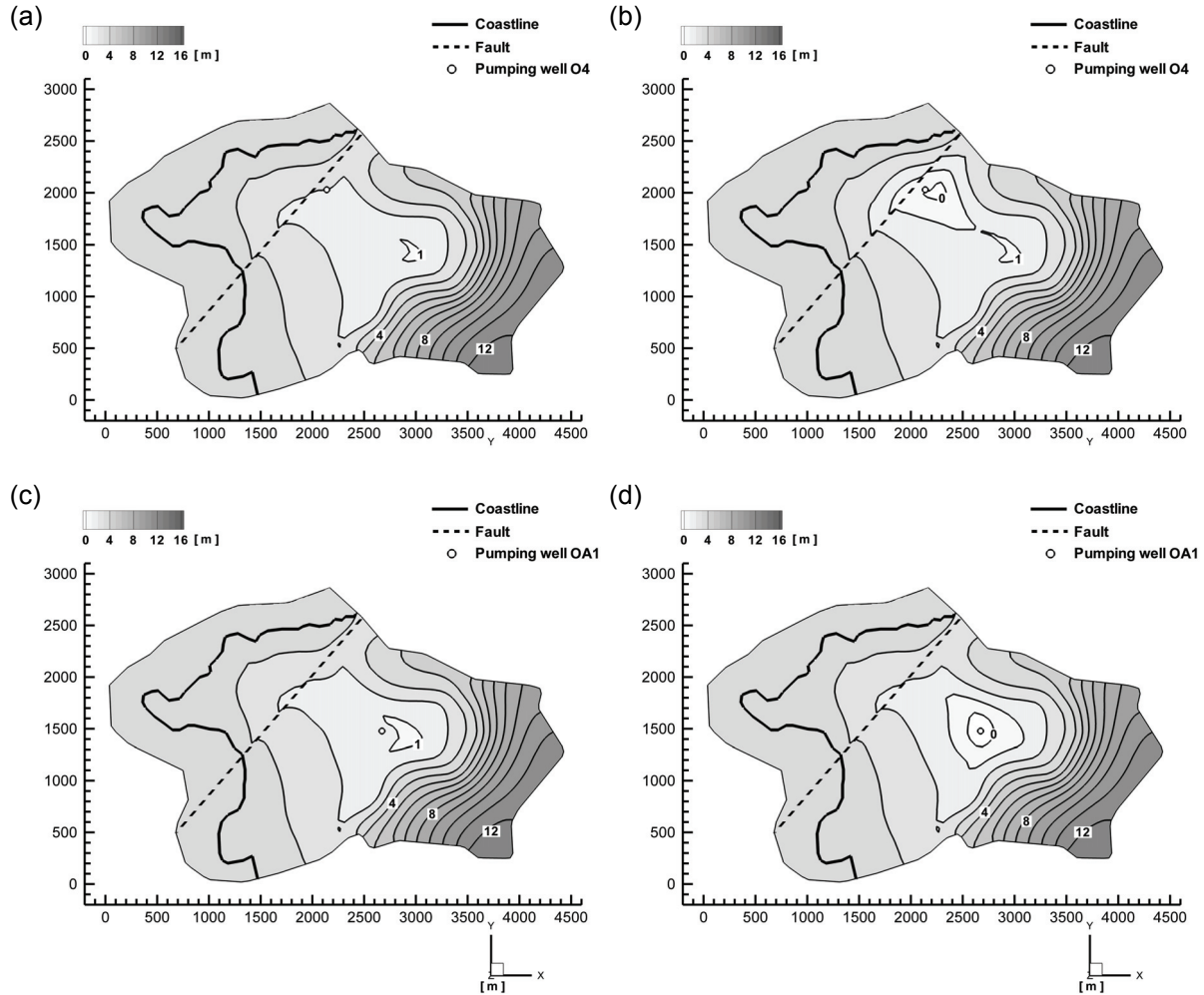


**Fig. 6** Final steady-state spatial distributions of hydraulic head (m) at the bottom boundary during groundwater pumping at rates of: (a) 100 m<sup>3</sup>/day at Well O4, (b) 400 m<sup>3</sup>/day at Well O4, (c) 100 m<sup>3</sup>/day at Well OA1, and (d) 400 m<sup>3</sup>/day at Well OA1 in the coastal aquifer system. The contour interval of hydraulic head is 1 m.

increases even after that at Well OA1 reaches its final steady-state condition. It strongly suggests that the major fault influences and controls more highly density-dependent groundwater flow and salt transport when groundwater is pumped from Well O4 as it is closer to the major fault than Well OA1. As shown in Figs 4–9, the major fault acts as a highly permeable conduit along it but behaves as a less permeable barrier across it. As a result, it retards seawater intrusion toward Well O4.

## CONCLUSIONS

Using a multidimensional hydrodynamic dispersion numerical model, density-dependent groundwater and salt transport before and during groundwater pumping in an unsaturated fractured porous coastal aquifer system, which is heterogeneous and true anisotropic, were simulated, validated, predicted, and analysed. The coastal aquifer system is composed of Quaternary alluvial layers underlain by Precambrian

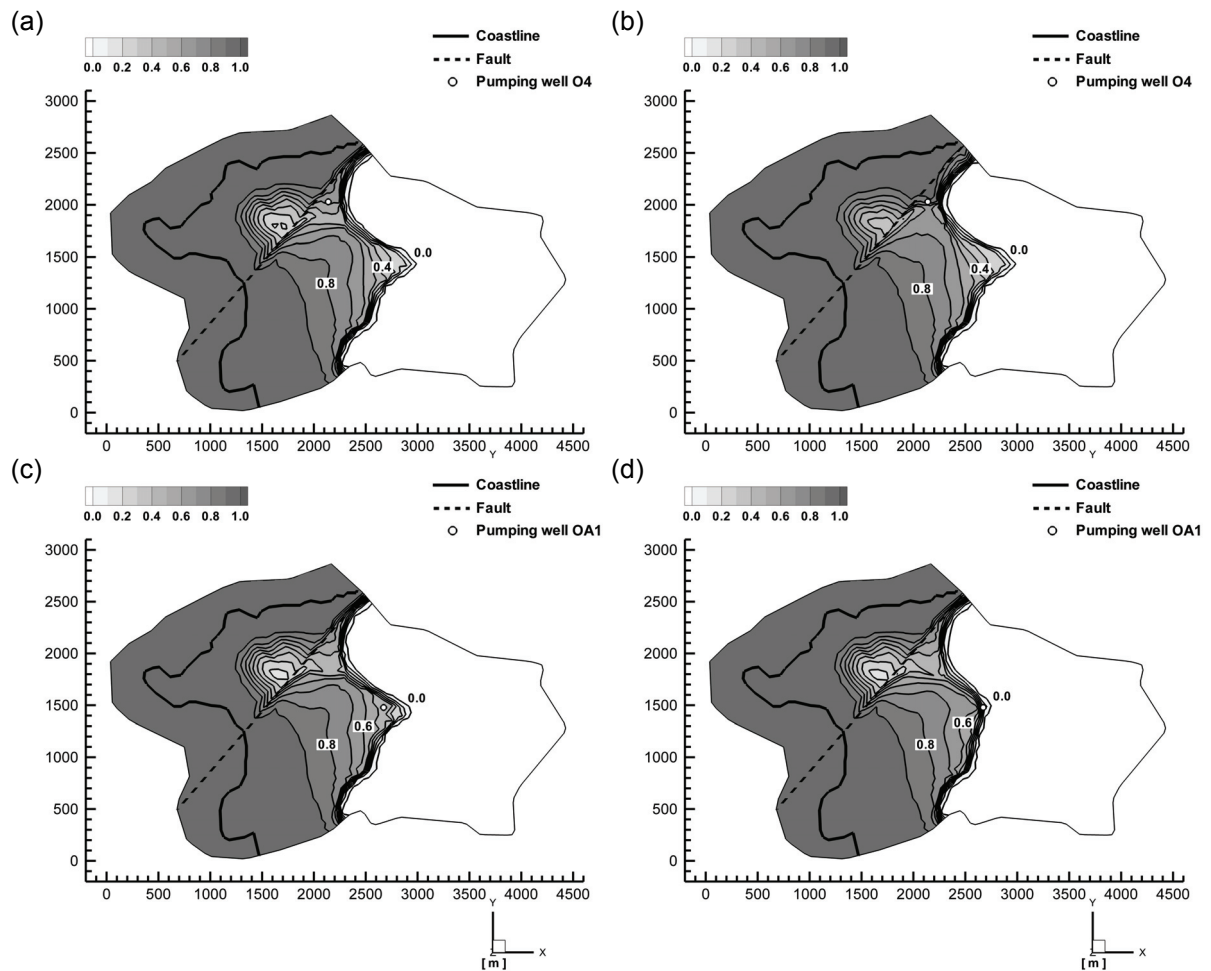


**Fig. 7** Final steady-state spatial distributions of normalized salt concentration at the bottom boundary during groundwater pumping at rates of: (a)  $100 \text{ m}^3/\text{day}$  at Well O4, (b)  $400 \text{ m}^3/\text{day}$  at Well O4, (c)  $100 \text{ m}^3/\text{day}$  at Well OA1, and (d)  $400 \text{ m}^3/\text{day}$  at Well OA1 in the coastal aquifer system. The contour interval of normalized salt concentration is 0.1.

gneiss and Cretaceous quartz monzonite, rhyolitic tuff, Kyokpori Formation (conglomerate, sandstone, and shale), and rhyolite with a major fault. A steady-state numerical simulation was performed first to obtain initial steady-state spatial distributions of density-dependent groundwater flow and salt transport before groundwater pumping, and its results were illustrated and validated reasonably with respect to the measured transition zones between fresh water and salt water. Four different transient-state numerical simulations were then performed to obtain spatial and temporal distributions of density-dependent groundwater flow and salt transport during groundwater pumping at two different pumping wells and two different pumping rates, and their results were illustrated and analysed. These steady and transient-state numerical simulation results show that such heterogeneity and true anisotropy have significant effects on spatial and temporal distributions of density-dependent groundwater flow and salt transport. Therefore, it may be concluded that both heterogeneity and true anisotropy cannot always be ignored if they are observed

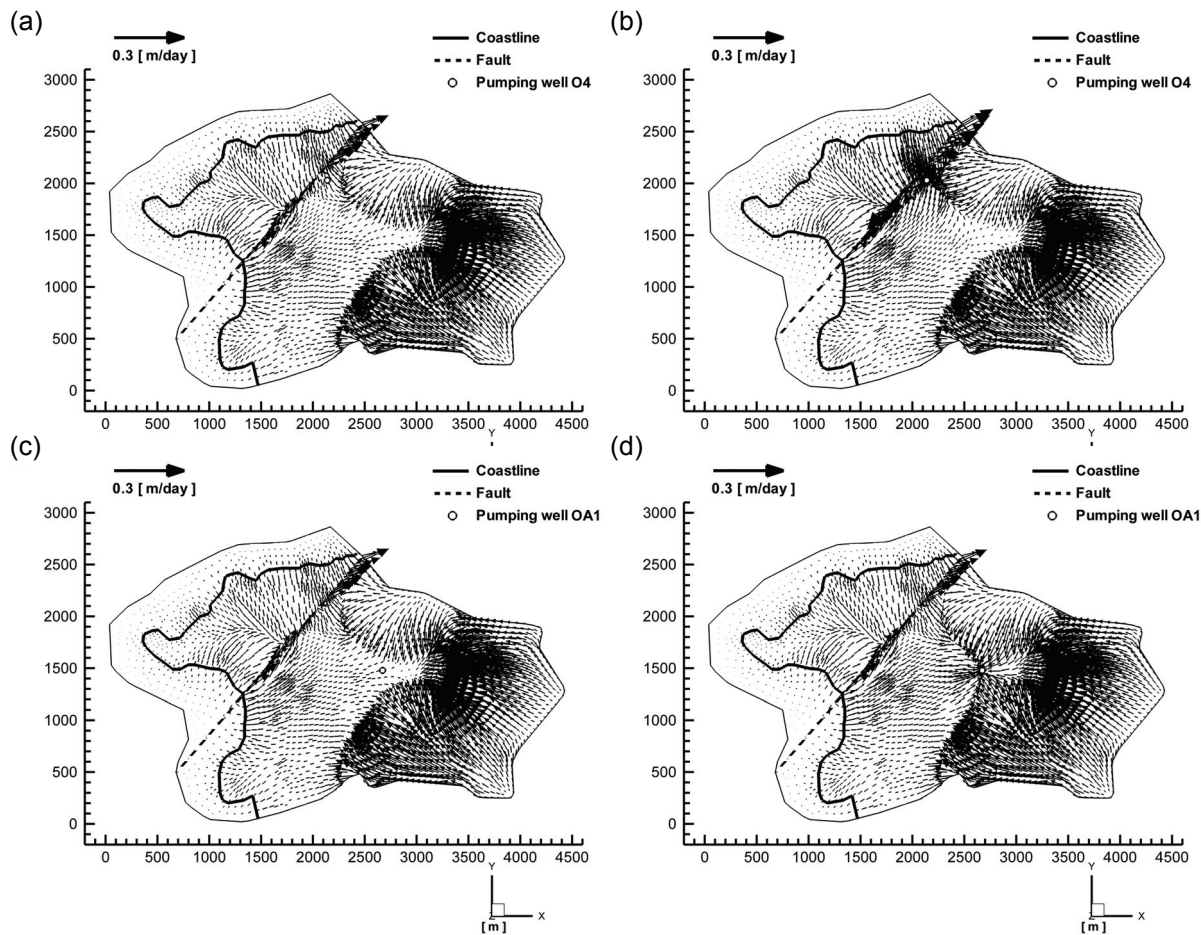


**Fig. 8** Final steady-state spatial distributions of groundwater flow flux (m/day) at the bottom boundary during groundwater pumping at rates of: (a) 100 m<sup>3</sup>/day at Well O4, (b) 400 m<sup>3</sup>/day at Well O4, (c) 100 m<sup>3</sup>/day at Well OA1, and (d) 400 m<sup>3</sup>/day at Well OA1 in the coastal aquifer system.

in actual aquifer system, and thus they must be properly considered when more rigorous and reasonable predictions of long-term density-dependent groundwater flow and salt transport induced by groundwater pumping are to be obtained for the optimal management of coastal groundwater resources. Further numerical studies of various geologic and hydrogeological settings and field applications are recommended to arrive at more general conclusions concerning the effects of heterogeneity and true anisotropy on three-dimensional density-dependent groundwater flow and salt transport due to groundwater pumping in unsaturated fractured porous aquifer systems.

**Acknowledgements** This work was supported by the Sustainable Water Resources Research Center of the 21st Century Frontier Research and Development Program, Ministry of Science and Technology, Korea. This work was also supported in part by the Brain Korea 21 Project, Ministry of Education and Human Resources Development, Korea.

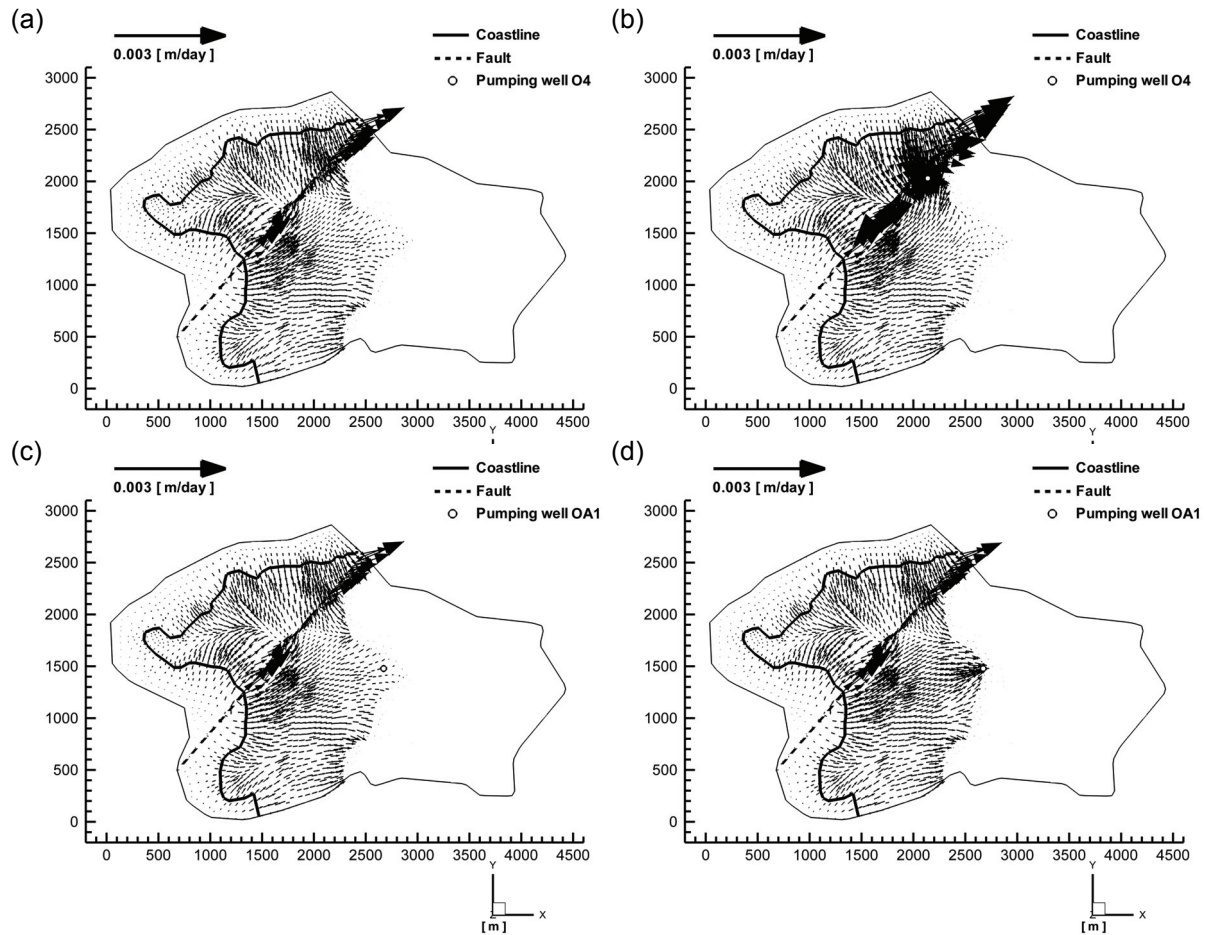


**Fig. 9** Final steady-state spatial distributions of normalized salt transport flux (m/day) at the bottom boundary during groundwater pumping at rates of: (a) 100 m<sup>3</sup>/day at Well O4, (b) 400 m<sup>3</sup>/day at Well O4, (c) 100 m<sup>3</sup>/day at Well OA1, and (d) 400 m<sup>3</sup>/day at Well OA1 in the coastal aquifer system.

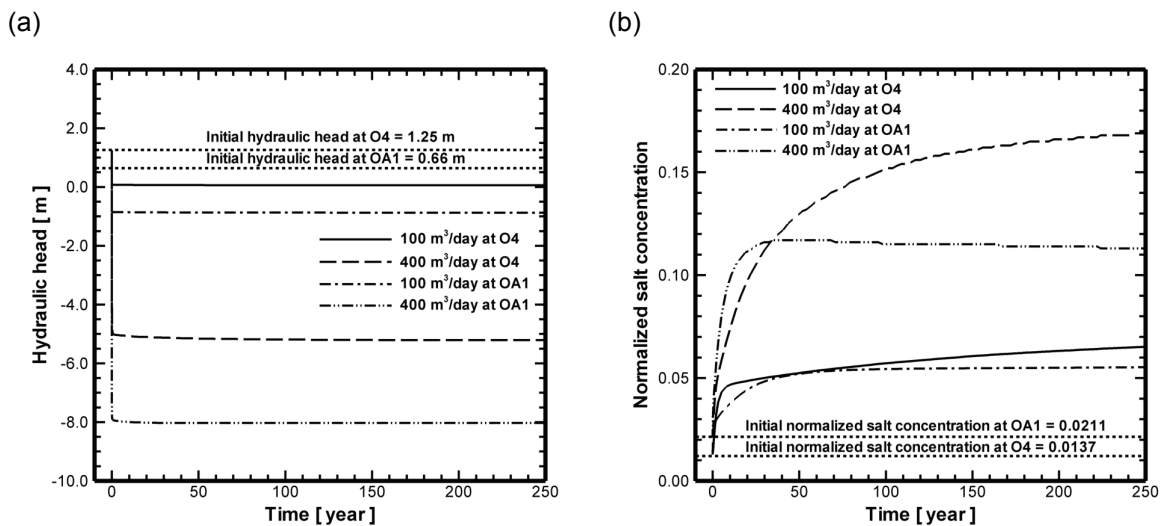


**Fig. 10** Temporal changes of: (a) hydraulic head (m) and (b) normalized salt concentration at Wells O4 and OA1 during groundwater pumping at 100 and 400 m<sup>3</sup>/day in the coastal aquifer system.

## REFERENCES

- Bear, J., Cheng, A. H. D., Sorek, S., Ouazar, D. & Herrera, I. (1999) *Seawater Intrusion in Coastal Aquifers: Concepts, Methods, and Practices*. Kluwer Academic Publishers, Norwell, Massachusetts, USA.
- Cheng, A. H. D. & Ouazar, D. (2004) *Coastal Aquifer Management: Monitoring, Modeling, and Case Studies*. Lewis Publishers, Boca Raton, Florida, USA.
- Domenico, P. A. & Schwartz, F. W. (1990) *Physical and Chemical Hydrogeology*. John Wiley and Sons, New York, USA.
- Fetter, C. W. (1994) *Applied Hydrogeology*, third edn. Prentice Hall, Upper Saddle River, New Jersey, USA.
- Freeze, R. A. & Cherry, J. A. (1979) *Groundwater*. Prentice Hall, Englewood Cliffs, New Jersey, USA.
- Kim, J. M. (2006) Development and application of a hydrodynamic dispersion numerical model for coastal groundwater management. Final Report, Geological and Groundwater Engineering Laboratory, Seoul National University, Seoul, Korea.
- Kim, S. B. (2000) Sedimentary processes and environments of the Kyokpori Formation (Cretaceous), SW Korea. PhD Thesis, Seoul National University, Seoul, Korea.
- Kim, J. M. & Yeh, G. T. (2004) COFAT3D: a finite element model for fully coupled groundwater flow and solute transport in three-dimensional saturated-unsaturated porous and fractured media, version 1.0. Technical Report, Geological and Groundwater Engineering Laboratory, Seoul National University, Seoul, Korea.
- Korea Institute of Geoscience and Mineral Resources (1997) *Geological Map of Kwangju Area (1:250000)*. Korea Institute of Geoscience and Mineral Resources, Daejeon, Korea.
- Korea Meteorological Administration (1971–2000) Climatological data of Kunsan, Korea. Annual Report. Korea Meteorological Administration, Seoul, Korea (published annually and available from <http://www.kma.go.kr>).
- van Genuchten, M. Th. (1980) A closed-form equation for predicting the hydraulic conductivity of unsaturated soils. *Soil Sci. Soc. Am. J.* **44**(5), 892–898.
- Yeh, G. T., Cheng, J. R. & Cheng, H. P. (1994) 3DFEMFAT: Users' manual of a 3-dimensional finite element model of density-dependent flow and transport through saturated-unsaturated media, version 2.0. Technical Report, Department of Civil and Environmental Engineering, Pennsylvania State University, University Park, Pennsylvania, USA.